J. Fluid Mech. (1967), *vol.* 30, *part* 2, *pp.* 305–328
Printed in Great Britain

The Toms phenomenon: turbulent pipe flow of dilute polymer solutions

By P. S. VIRK, E. W. MERRILL, H. S. MICKLEY, K. A. SMITH

Department of Chemical Engineering, Massachusetts Institute of Technology, Cambridge, Massachusetts

AND

E. L. MOLLO-CHRISTENSEN

Department of Meteorology, Massachusetts Institute of Technology, Cambridge, Massachusetts

(Received 26 January 1967 and in revised form 20 April 1967)

Drag reduction caused by dilute, distilled water solutions of five polyethylene oxides, molecular weights from 80,000 to 6,000,000, in turbulent pipe flow was studied experimentally in 0·292 and 3·21 cm ID pipes. It was found that the onset of drag reduction occurs at a well-defined wall shear stress related to the random-coiling effective diameter of the polymer. Laminar to turbulent transition is not, in general, delayed. The extent of drag reduction induced by a homologous series of polymers in a given pipe is a universal function of concentration, flow rate, and molecular weight. The maximum drag reduction possible is limited by an asymptote that is independent of polymer and pipe diameter. Flow structure measurements in a single polymer solution, 1000 ppm of molecular weight 690,000, showed that the mean flow follows an 'effective slip' model. In this, the mean velocity profile consists of a 'Newtonian plug' convected along at an additional, 'effective slip' velocity. The turbulent flow structure follows the 'effective slip' model towards the pipe wall, but is significantly different from Newtonian towards the pipe axis; in particular, the inertial subrange observed in isotropic Newtonian turbulence was absent in an energy spectrum taken on the pipe axis in the polymer solution.

1. Introduction

Under certain conditions of turbulent pipe flow, dilute polymer solutions require a smaller specific energy expenditure than the pure solvent: thus with the polymer solutions, a lower pressure gradient is needed to maintain the same flow rate, or a higher flow rate can be attained for the same pressure gradient as solvent. This specific energy—or drag—reduction is termed the Toms phenomenon, after Toms (1948), who was the first to recognize it. The observations of Toms have been confirmed in many subsequent 'gross flow', pressure gradient *vs.* flow rate, studies (Fabula 1963; Savins 1964; Metzner & Park 1964; Hershey & Zakin 1965) with several different polymer-solvent systems in turbulent flow through pipes ranging from 0·1 to 5·0 cm ID. From these, two general aspects have been recognized. First, that the onset of drag reduction occurs in a fairly well-defined manner (Virk, Merrill, Mickley & Smith 1965; Hershey & Zakin 1965) and

second that, qualitatively, the extent of drag reduction increases with increasing flow rate, increasing polymer molecular weight and, within limits, increasing polymer concentration.

Four types of explanations, all unconfirmed and speculative, have been proposed for the Toms phenomenon.

(i) 'Effective' slip (Oldroyd 1948).

(ii) Inherently delayed laminar-to-turbulent transition (Savins 1964).

(iii) 'Anisotropic viscosity' (Shin 1965).

(iv) Visco-elasticity (Savins 1964; Metzner & Park 1964; Hershey & Zakin 1965).

The present work is an experimental investigation of the Toms phenomenon, performed with dilute solutions of a homologous series of linear, random-coiling polymers to determine the relation of polymeric parameters to drag reduction induced and the flow structure, mean and turbulent, prevailing when the phenomenon occurs.

2 Experimental

Two experimental pipe flow systems were employed. The majority of gross flow (flow rate *vs.* pressure gradient) measurements were made in a once-through blowdown system with a 0·292 cm ID pipe, 250 diameters long. Corroborative gross flow and all flow structure measurements were made in a recirculating system using a 3·21 cm ID test pipe, 475 diameters long. Pitot tubes were used for mean velocity profiles and a constant temperature anemometer with cylindrical, quartz-coated, hot film sensors for turbulent intensity and energy spectrum measurements. The flow in the 3·21 cm pipe was probed at its downstream end with a micrometer traverse capable of holding a Pitot tube and a hot film probe simultaneously in an 'over and under' arrangement; this permitted *in situ* calibration of the hot film before and after each set of turbulence measurements, enhancing their accuracy.

In both systems, flow rates could be varied to provide wall shear stresses from 1 to 2000 dynes/cm^2. In the 0·292 cm system, Reynolds numbers for laminar to turbulent transition were determined by introducing a disturbance at the pipe entrance via an external tap for 'natural' or a concentric 0·15 cm ID orifice for artificially 'triggered' transition. When the flow was critical, the disturbance was amplified and could be detected by a pressure transducer mounted downstream.

Five homologous polyethylene oxides, molecular weights from 80,000 to 6,000,000, were used with distilled water for solvent. Polymer concentration was varied from 0·5 to 5000 weight parts per million; in all cases polymer solution density was the same as that of the solvent and the maximum relative viscosity reached was around two. All experiments were performed at 25·0 $\pm$ 0·5 °C.

The polymer solutions used were prepared by dilution from concentrated master batches which were characterized by intrinsic viscosity measurements. Polymer molecular weight and r.m.s. radius of gyration were derived from the intrinsic viscosity using experimental relations for the polyethylene oxide–water system (Shin 1965).

Experimental apparatus and procedures have been described in detail elsewhere (Virk 1966).

3. Results and discussion: gross flow

In both systems, flow rate, Q, *vs.* wall shear stress, T_w, results with pure solvent agreed well with established Newtonian friction factor relations, Poiseuille's in laminar and Prandtl's in turbulent flow, and were highly reproducible; the 99 % confidence belt on the wall shear stress was everywhere within ± 1 % of the absolute value. In the 0·292 cm system the critical Reynolds number was 3150 ± 230 for 'natural' and 2025 ± 70 for 'triggered' transition.

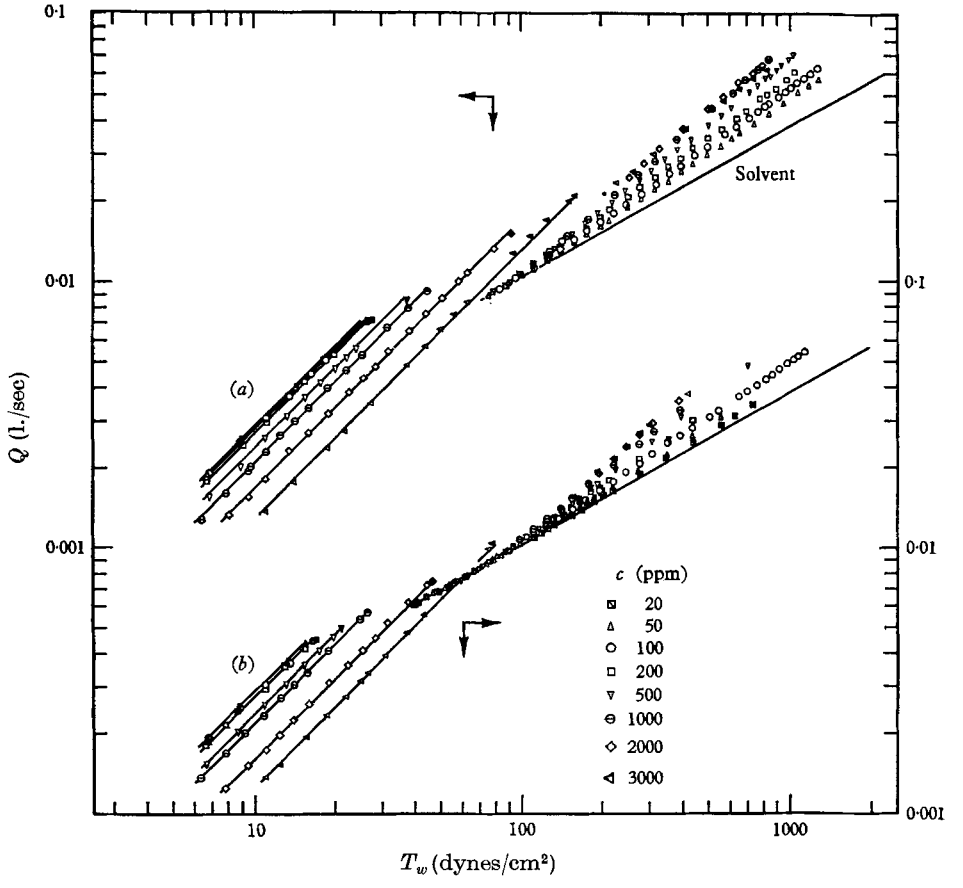

FIGURE 1. Typical flow diagrams in 0·292 cm pipe; (*a*) without trigger, (*b*) with trigger. Polymer: N 750. Solid points indicate transition.

Figures 1 and 2 show typical polymer solution gross flow diagrams. Four distinct regimes are observed:

(i) the laminar regime,
(ii) the transition region,
(iii) turbulent flow, without drag reduction,
(iv) turbulent flow, with drag reduction.

A striking feature is the sharp division between regions (iii) and (iv). For a given polymer-solvent combination the wall shear stress, T_w^*, at this point, which marks the onset of drag reduction, is constant over large ranges of concentration; further, it appears independent of pipe diameter. T_w^* decreases with increasing polymer molecular weight. Region (iv) is characteristic of the Toms phenomenon; throughout it, polymer solution flow lines (Q *vs.* T_w) lie to the left of the solvent line, indicative of lower specific power consumption. At constant concen-

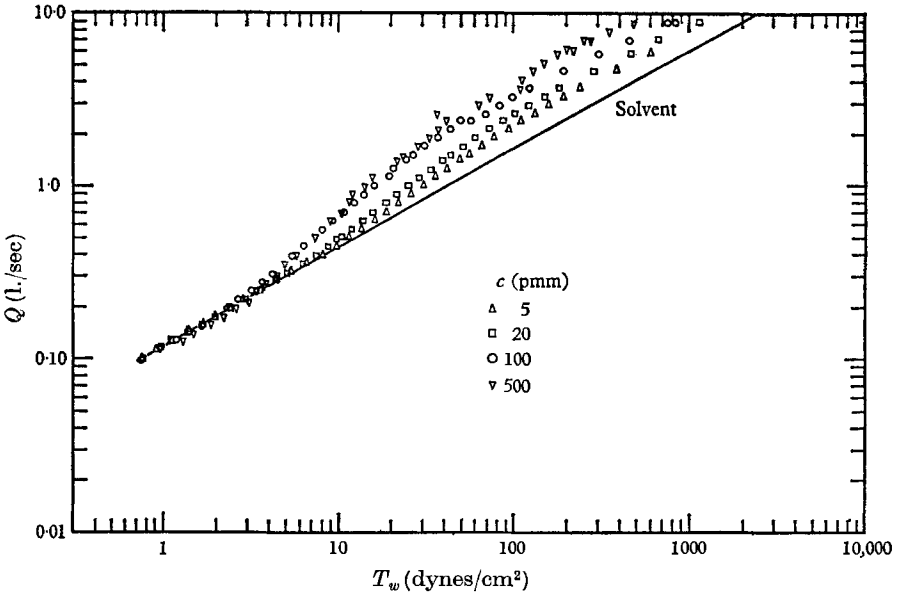

FIGURE 2. Typical flow diagrams in 3·21 cm pipe. Polymer: W 301.

tration, the flow lines diverge from the solvent line so that drag reduction increases with flow rate. For a given polymer this divergence increases with increasing concentration initially but eventually becomes independent of concentration. Correspondingly, the fractional drag reduction, R_F, increases initially with increasing concentration but tends to a constant, maximum value $R_{F,\max}$, at high concentrations. Two asymptotes limit the maximum drag reduction that can be attained. One is the high concentration asymptote noted above; its slope Np ($= d\ln T_w/d\ln Q$) is a function of polymer and approaches unity with increasing molecular weight. The other is a polymer-independent asymptote, beyond which the wall shear stress could never be reduced; its slope, Nm, is about $\frac{3}{2}$ in both pipes. This latter is shown on figure 3; in several cases the marked change in slope from Np to Nm may be observed as the flow lines switch asymptotes. The maximum fractional drag reductions achieved were about 0·65 in the 0·292 cm and 0·80 in the 3·21 cm systems.

The laminar regime

All polymer solutions tested were Newtonian, i.e. obeyed Poiseuille's law, in laminar flow. Also, for each polymer the relative viscosities for various concentrations yielded a high shear rate ($\simeq 10^3\,\mathrm{sec}^{-1}$) intrinsic viscosity which was the

same as that obtained independently in a low shear ($\simeq 10^0 \text{sec}^{-1}$) laminar Couette viscometer. The absence of non-Newtonian effects—notably the 'shear thinning' commonly associated with polymer solutions—is due to the relative diluteness of the present solutions even at the highest concentrations employed.

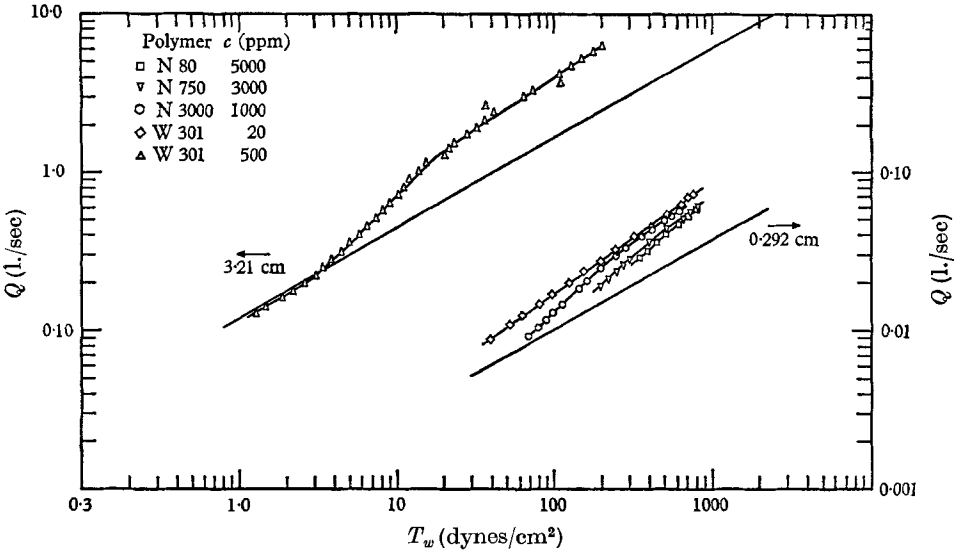

FIGURE 3. Asymptotic slopes in 0·292 and 3·21 cm pipes for four polyethylene oxide polymers.

The onset of drag reduction

The abruptness of the onset of drag reduction suggests that a necessary condition exists, explicitly connecting the macromolecule causing the Toms phenomenon to the turbulent shear flow in question, which must be satisfied for drag reduction to occur. The Onset Hypothesis, presented in an earlier work (Virk *et al.* 1965), is an attempt to relate macromolecular diameter to a dissipative turbulence scale at onset. The hypothesis is recounted very briefly.

From two standpoints (Tanford 1961), the thermodynamic 'excluded volume' and the hydrodynamic 'equivalent Einsteinian sphere', the effective diameter, D_M, of a random coiling macromolecule in dilute solution is about twice its rms radius of gyration, R_G, independent of concentration. So

$$D_M = 2R_G. \tag{1}$$

Polymer solutions are considered dilute as long as the conformation of an individual macromolecule is unaffected by its neighbours: this corresponds, roughly, to the volume fraction of macromolecules based on D_M being less than that for random spherical packing.

Drag reduction is an 'energetic' phenomenon and the rates of dissipation and production of turbulent energy are known to show sharp maxima at $y^+ \simeq 10$; y^+ being the usual dimensionless distance from the wall. Therefore, the parameter chosen to characterize the turbulence was a 'dissipation wave-number', k_d, derived from a turbulent energy spectrum close to the wall and defined as the

wave-number where the dissipation, $k^2E(k)$, is a maximum. Thus k_d is a measure of the 'fine' scale of turbulence at which the dissipation of turbulent energy occurs. By invoking existing turbulence theory (Hinze 1959) and experiment (Laufer 1954), it can be shown that

$$k_d = Ku_\tau/\nu, \tag{2}$$

where K is a constant, of order 10^{-1}, that depends only on y^+: at $y^+ \simeq 10$ the best estimate is $K \approx 0{\cdot}2$. u_τ is the friction velocity, $(T_w/\rho)^{\frac{1}{2}}$, and ν the kinematic viscosity.

The Onset of Drag Reduction Hypothesis states that: the onset of drag reduction in the turbulent flow of dilute polymer solutions occurs at a constant value of the product $D_M k_d^*$ which is a ratio of the dimensions of the macromolecule and the fine scale of the turbulent shear flow. So

$$D_M k_d^* = C, \tag{3}$$

where C is a universal dimensionless constant and the asterisk indicates a value taken at onset. Using (2),

$$D_M(u_\tau^*/\nu) = C'; \quad C' = C/K \tag{4}$$

from which, for a given polymer homologous series and solvent,

$$(T_w^*)^{\frac{1}{2}} = C''/R_G; \quad C'' = \tfrac{1}{2}C'\nu\rho^{\frac{1}{2}}. \tag{5}$$

The Onset Hypothesis has the following consequences.

(i) From (1), for a given macromolecule-solvent, $(T_w^*)^{\frac{1}{2}}$ should be independent of concentration for dilute solutions.

(ii) From (2), for a given macromolecule-solvent, $(T_w^*)^{\frac{1}{2}}$ should be independent of pipe diameter.

(iii) In any pipe, from (4), (u_τ^*/ν) should vary as $(1/D_M)$, or, from (5), for a given homologous series and solvent, $(T_w^*)^{\frac{1}{2}}$ should vary inversely as R_G.

(iv) The onset constant, C (and C') should be universally constant, regardless of pipe, solvent and macromolecule.

These consequences were shown to hold reasonably with four polymers in the 0·292 cm pipe (Virk *et al.* 1965); in the present work the results are extended to five polymers and both 0·292 and 3·21 cm pipes. The validity of consequence (i) has already been noted; error analysis of the present results shows that, typically, $(T_w^*)^{\frac{1}{2}}$ is constant to within $\pm 10\,\%$ over 100-fold ranges of concentration. Figure 4 shows that both consequences (ii) and (iii) hold; results from both pipes, differing 11-fold in diameter, straddle the same straight line over an 8-fold range of R_G and, within experimental error, the line passes through the origin as predicted by (5). Verification of consequence (iv) requires considerably more experimental information than currently available in the literature. The existing onset data that can be analysed is summarized in table 1 from which $C' = (D_M u_\tau^*/\nu)$ is $0{\cdot}015 \pm 0{\cdot}005$. From this value of C' the onset wall shear stress for any characterized polymer-solvent pair can be predicted empirically.

Values of C' and K lead to an onset constant, $C = D_M k_d^*$, which should physically be the ratio of macromolecule to dissipative eddy size at onset, of $0{\cdot}003 \pm$

0·001. In regard to this surprisingly low value it must be pointed out that while R_G and u_τ/ν are basic macromolecular and turbulence scales respectively, the constants which convert these to universal physical entities are somewhat uncertain. For example, R_G is a statistical average and even an externally unperturbed macromolecule will, on occasion, assume extended configurations. Also, random coiling macromolecules are subject to deformation under shear and will,

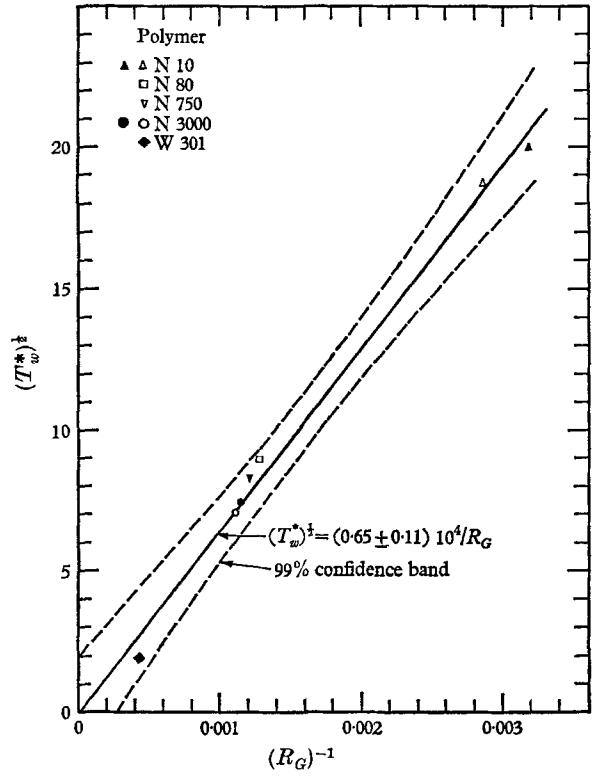

FIGURE 4. The Onset Hypothesis. T_w^* is in dynes/cm², R_G in Å. Hollow and solid points were derived from 0·292 and 3·21 cm pipes respectively. (In order of decreasing $(T_w^*)^{\frac{1}{2}}$, points on figure refer to entries 1 to 7 on table 1.)

consequently, suffer both mean and transient elongations in a turbulent pipe flow. On both these counts, however, calculations (based on Flory (1953) and Peterlin (1960) respectively) show that the maximum extensions expected are of order unity. Thus, even if the onset of drag reduction reflects an interaction of the turbulence with extended modes of the macromolecule, no order of magnitude error is incurred by the direct use of the zero-shear r.m.s. radius of gyration, R_G, in the macromolecular length D_M. With respect to the turbulence, k_d was chosen as the wave-number with the maximum local energy dissipation rate. In practice, the energy dissipation occurs over a two-decade range of wave-numbers with a relatively flat maximum. The highest wave-number, k_e, that might be associated with dissipation (defined, for example, such that 95% of the total dissipation occurs at $k < k_e$), is typically of order $10\,k_d$. Thus if onset is characterized by the

interaction of the macromolecule with the highest dissipative wave-numbers (i.e. the smallest dissipative eddies) rather than the wave-numbers of maximum dissipation, the resultant macromolecule to dissipative eddy ratio, $D_M k_e^*$, would be roughly an order of magnitude higher than $D_M k_d^*$. Further, owing to the unavail-

No.	Polymer-solvent system	$[\eta]$ (dl./g)	$M \times 10^{-6}$	D (cm)	R_G (Å)	(u_τ^*/ν) (cm^{-1})	C'	Present polymer designation
1	PEO–water	0·66	0·080	3·21	315	2240	0·0141	N 10
2		0·73	0·092	0·292	350	2100	0·0147	N 10
3		1·75	0·28	0·292	795	1000	0·0159	N 80
4		3·38	0·63	0·292	835	940	0·0157	N 750
5		3·61	0·69	3·21	875	830	0·0145	N 3000
6		3·90	0·76	0·292	910	790	0·0144	N 3000
7		20·1	6·1	3·21	2350	210	0·0099	W 301
8	PMMA–MCB	3·90	2·3	0·128	600	1030	0·0124	—
9		3·90	2·3	0·404	600	1100	0·0132	—
10	PIB–CYC	3·44	0·72	0·081	445	2190	0·0195	—
11		3·44	0·72	0·117	445	2200	0·0196	—
12		3·44	0·72	1·29	445	2320	0·0206	—
13		3·44	0·72	2·54	445	1660	0·0148	—
14	PIB–BEN	0·82	0·72	1·29	275	3740	0·0206	—
15		0·82	0·72	2·54	275	2640	0·0145	—

Abbreviations used are:

PMMA, polymethylmethacrylate — MCB, monochlorobenzene
PIB, polyisobutylene — CYC, cyclohexane
PEO, polyethylene oxide — BEN, benzene

Sources: nos. 1 to 7 from present work, 8, 9 from Toms (1948), 10 to 15 from Hershey & Zakin (1965).

R_G values: nos. 1 to 7 experimental (Shin 1965), 8 to 15 calculated (via Flory 1953).

ν is for the solvent in all cases.

TABLE 1. Summary of experimental onset of drag reduction data.

ability of experimental energy spectra in the vicinity of $y^+ \simeq 10$, the value used for K in (2) was derived from a spectrum at $y^+ = 72$ (Laufer 1954) and could be somewhat low. Thus, the relevant macromolecule/eddy ratio could be between one and two orders of magnitude higher than the computed value of C, but this is speculation; it is clear that the physical interpretation of the onset constant, C, must await clarification of the mechanism of macromolecule–turbulence interaction and the procedures for scaling the turbulence. Needless to add, the above considerations do not affect the empirical onset constant, C'.

The Onset Hypothesis is based on length scales. On entirely analogous grounds one may postulate a time-based hypothesis, substituting macromolecular terminal relaxation time, τ_M, for D_M and a dissipation frequency, ω_d, for k_d. τ_M may be calculated from linear visco-elastic theory (e.g. Zimm 1956) and ω_d can be scaled by (u_τ^2/ν), whence the time-based analogue of (4) is

$$\tau_M(u_\tau^{*2}/\nu) = C_t'. \tag{6}$$

The time-based hypothesis is evaluated in table 2 for the data presented on table 1. Its failure is evident: values of C_t' vary 100-fold over the range that the length constant, C', was constant within $\pm 30\,\%$. Recently, a time hypothesis has been proposed (Hershey & Zakin 1965) and compared with data obtained from two polymer-solvent systems in several pipes. Analysis of the two systems, polyisobutylene ($M = 0{\cdot}72 \times 10^6$) in cyclohexane and polymethylmethacrylate ($M = 1{\cdot}5 \times 10^6$) in toluene, reveals, however, that the terminal relaxation times (and the radii of gyration) were nearly identical.

No.	τ_M (sec $\times 10^3$)	(u_τ^{*2}/ν) (sec$^{-1} \times 10^{-3}$)	C_t'
1	0·00081	45·0	0·036
2	0·0010	39·5	0·040
3	0·0074	8·9	0·066
4	0·033	7·9	0·256
5	0·038	6·2	0·235
6	0·045	5·6	0·254
7	1·86	0·39	0·733
8	0·17	7·3	1·21
9	0·17	8·3	1·38
10	0·054	54·5	2·97
11	0·054	55·0	3·00
12	0·054	61·0	3·33
13	0·054	31·0	1·71
14	0·0089	98·0	0·87
15	0·0089	49·0	0·43

Serial no. of entries is same as in table 1.
τ_M is terminal relaxation time calculated from Zimm theory (Zimm 1956).

TABLE 2. Test of the time based onset hypothesis.

Transition

Both with and without the trigger, the majority of polymer solutions tested did not delay transition, as shown on figure 5. The few cases that did cause a delay satisfied the criterion that the wall shear stress, $T_{w,T}$, corresponding to the normal (solvent) transition Reynolds number, $N_{Re,T}$, exceeded the onset wall shear stress, T_w^*. This delay criterion, $T_{w,T} > T_w^*$, must be viewed cautiously because of the method of measurement. In this, the flow was disturbed at the entrance; when it was critical, this disturbance caused a turbulent 'patch' to travel downstream. The pressure gradient in the turbulent patch would be much greater than in a laminar flow (at the same flow rate), so when this patch passed the static pressure taps downstream, a larger pressure differential would prevail, momentarily, across them, causing the pressure transducer to 'hiccup'. Now if the dissipation in the turbulent patch were reduced—and, from the Onset Hypothesis, this will occur only when $T_{w,T} > T_w^*$—then the transducer might fail to see the patch, even though it was, technically, turbulent. There is a possibility, therefore, that the cases of apparent delay were not truly delayed. Taken with the absence of a delay in the majority of the cases, this would imply that

the polymer solutions *never* delay transition. Hot wire studies, which would directly determine turbulence, are planned to resolve the matter.

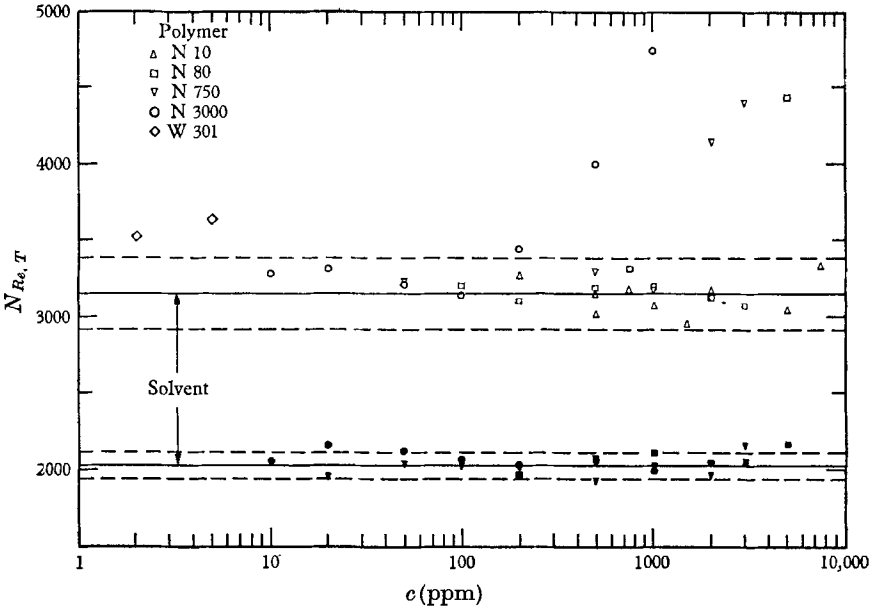

FIGURE 5. Laminar-to-turbulent transition in 0·292 cm pipe. Solid points are with trigger; dashed lines are 99 % confidence limits for solvent $N_{Re,T}$.

The extent of drag reduction

Polymer dependent factors

The fractional drag reduction, R_F, is defined by

$$R_F = (1-(T_{wp}/T_{ws}))_Q, \tag{7}$$

where T_{wp} and T_{ws} are the wall shear stresses in polymer solution and solvent respectively at flow rate Q. The specific drag reduction, R, for polymer concentration c is

$$R = R_F/c \tag{8}$$

which, at infinite dilution, yields the intrinsic drag reduction,

$$[R] = \lim_{c\to 0}(R), \tag{9}$$

$[R]$ is a measure of the drag reducing 'efficiency' of the initial increments of polymer. In the region of the Toms phenomenon (region (iv)), for a given polymer and flow rate, the specific drag reduction decreases monotonically with increasing concentration. These R *vs.* c curves have a characteristic shape which, in doubly-logarithmic co-ordinates, exhibits two straight-line asymptotes:

$$R = [R] \quad (c\to 0); \tag{10a}$$

$$R = R_{F,\max}/c \quad (c\to\infty). \tag{10b}$$

The intersection of these defines a characteristic, intrinsic, concentration,

$$[C] = R_{F\ \max}/[R]. \tag{11}$$

The limit $c \to \infty$ above is meant in a thermodynamic sense; it implies concentrated solutions.

Normalization of the co-ordinates of the R *vs.* c curves obtained in the 0·292 cm pipe by their respective parameters $[R]$ and $[C]$ (given in table 3) results, irrespective of polymer and flow rate, in their superposition onto a single universal drag reduction curve, figure 6. On it, the universal co-ordinates are

$$\gamma = c/[C], \tag{12a}$$

$$\delta = R/[R], \tag{12b}$$

Polymer	Q (l./sec)	$[R]$ (dl./g)	$[C]$ (g/dl.)
N 10	0·040	0·75	0·335
	0·050	1·2	0·235
N 80	0·040	35	0·0145
	0·050	46	0·0115
N 750	0·040	200	0·0029
	0·050	240	0·0025
N 3000	0·015	120	0·0040
	0·020	190	0·0030
	0·030	280	0·0022
	0·040	330	0·0020
	0·050	370	0·0018

The accuracy of all $[R]$ and $[C]$ values is estimated at ± 10 %. dl. is short for decilitres.

TABLE 3. Superposition parameters for the universal drag reduction curve (figure 6).

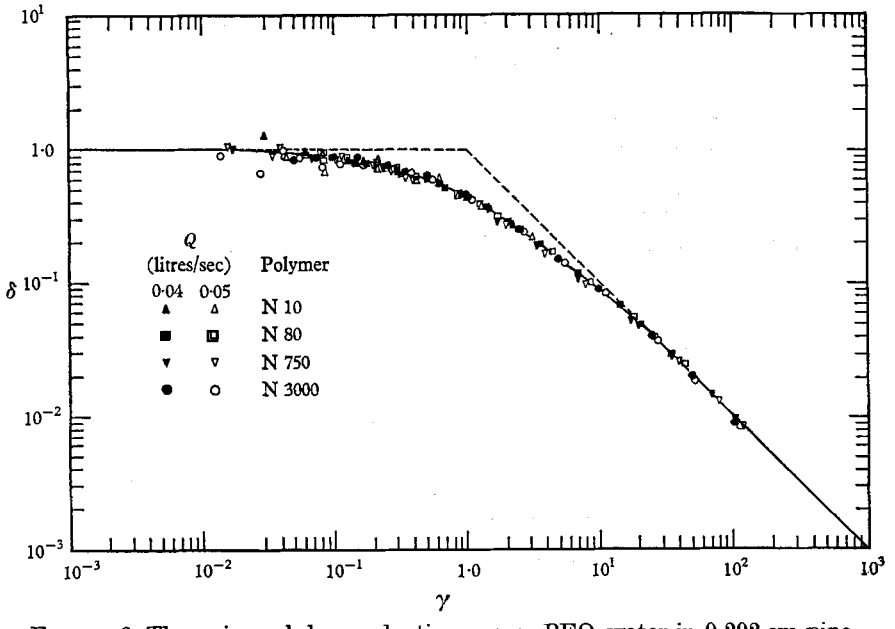

FIGURE 6. The universal drag reduction curve; PEO–water in 0·292 cm pipe. (Superposing constants $[R]$ and $[C]$ are given in table 3.)

and the universal curve itself is quite well represented by

$$\delta = 1/(1+\gamma). \tag{13}$$

The superposing parameters $[R]$ and $[C]$ are themselves uniquely related and each can be decomposed into flow rate and polymer dependent terms. Invoking the approximate logarithmic linearity of the flow lines, figures 1 and 2, and noting that the onset point (Q^*, T_w^*) is common to both solvent and polymer solutions, it can be shown that

$$[R] = \psi \ln (Q/Q^*); \quad \psi = -(dnp/dc)_{c\to 0}, \tag{14a}$$

$$[C] = (1-(Q/Q^*)^{(Np-ns)})/[R], \tag{14b}$$

where np and ns are the slopes, $(d \ln T_w/d \ln Q)$, of polymer solution and solvent flow lines respectively. The two polymeric extent of drag reduction parameters in equations (14) are the intrinsic function, ψ, characteristic of low concentrations

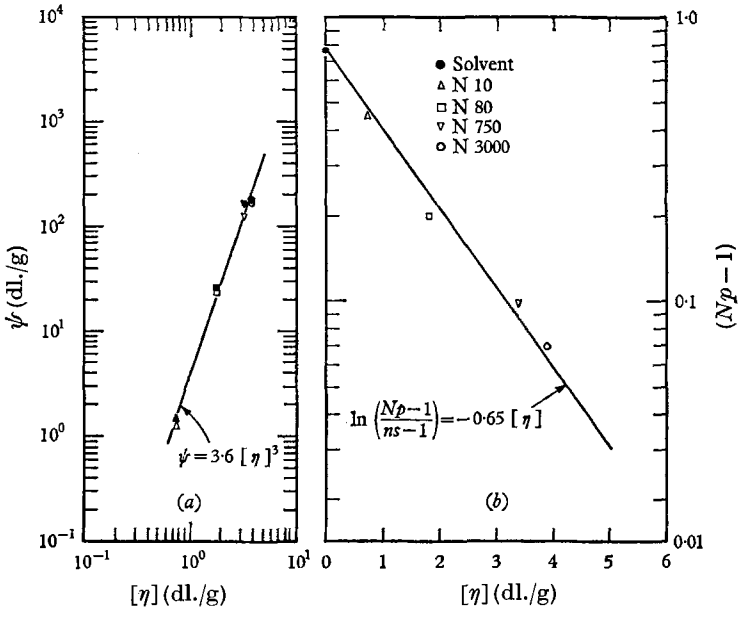

FIGURE 7. Polymeric extent of drag reduction parameters. (*a*) The intrinsic function ψ (same symbols as figure 6). (*b*) The polymer limited asymptotic slope, Np.

and the polymer-limited asymptotic slope, Np, characteristic of high concentrations. Experimental values of both correlate well with polymer intrinsic viscosity, $[\eta]$, as shown on figures 7 (*a*) and (*b*), though no physical significance can be attributed to either of the relations. The correlation cannot, at present, be extended to include the effect of pipe diameter, D, but it is suspected that the numerical constants in the $[\eta]$ *vs.* ψ and Np relations are functions of D. In general, at flow rates corresponding to equal solvent wall shear stress, the fractional drag reduction induced by a given concentration of polymer decreases with increasing pipe diameter.

Reversal of the foregoing analysis permits the entire drag-reducing behaviour of a homologous series and solvent in a given pipe and within the polymer-

dependent region to be synthesized as follows. From the Onset Hypothesis, (4), T_w^* can be predicted and, knowing pipe diameter, the onset point, (Q^*, T_w^*), ascertained. Next, from $[\eta]$ and relations such as those of figure 7, polymeric parameters ψ and Np can be obtained which lead, given the operating flow rate, Q, to values of $[R]$ and $[C]$ via equations (14*a*) and (14*b*) respectively. Finally, using the polymer concentration in question, a universal curve such as figure 6 or equation (13) is entered at $\gamma = c/[C]$ and the corresponding value of $\delta = R/[R]$ yields, via (8), the fractional drag reduction, R_F, to be expected. While the results of several other investigators (for example, Toms 1948; Fabula 1963) are qualitatively similar, no adequate data exist in the literature to test the correlations developed.

Polymer independent limitations

The maximum drag reduction asymptote, slope $Nm \simeq \frac{3}{2}$, noted in both pipes is shown plotted in the Prandtl form on figure 8; its universality, independent of pipe, polymer and concentration, is evident. Figure 8 sets the limits within which the Toms phenomenon is exhibited in smooth pipes; i.e. the solvent line followed prior to onset and the asymptote which eventually supercedes all flow lines, both being independent of polymer and universal in Newtonian coordinates, f and N_{Re}. In between these limits the flow lines depend on f, N_{Re}, the polymer, and its concentration. Comparison of the equivalent power law form of the asymptote with laminar and turbulent friction factor relations:

$$f = 16N_{Re}^{-1\cdot0} \quad \text{laminar (Poiseuille)}, \tag{15a}$$

$$f = 0\cdot079N_{Re}^{-0\cdot25} \quad \text{turbulent (Blasius)}, \tag{15b}$$

$$f = 0\cdot42_{Re}^{-0\cdot55} \quad \text{asymptote}, \tag{15c}$$

establishes that the ultimate condition of drag reduction in the Toms phenomenon is definitely not laminar flow. This maximum drag reduction asymptote has not hitherto been reported and positive literature confirmation is lacking though two investigators (Toms 1948; Metzner & Park 1964) appear to have attained it.

The Newtonian solvent

All onset and extent of drag reduction relations presented were developed with respect to the solvent. So long as the polymer solutions remain dilute, the viscosity build-up with increasing concentration can approximately be accounted for by referring all relations to the 'Newtonian' rather than the pure solvent; the former has the same viscosity as the polymer solution in question but obeys Newtonian flow relations (that is, exhibits no drag reduction). Its relative viscosity might be obtained from the Flory–Huggins expansion,

$$\eta_r = 1 + c[\eta] + 0\cdot35(c[\eta])^2 + \ldots. \tag{16}$$

Polymer degradation

Drag reduction by dilute polymer solutions is invariably accompanied by a decrease in polymer molecular weight—termed degradation. In the 0·292 cm

pipe without the trigger—from which most gross flow data were derived—polymer degradation was found, by intrinsic viscosity measurements, to be negligible. In the recirculating 3·21 cm system, degradation was slight before onset, $(Q/Q^*) < 1$, and very severe for $(Q/Q^*) > 10$; thus onset data were essentially unaffected, but extent of drag reduction data were not entirely suitable for correlation. Degradation does not affect final asymptote data as long as the concentration of undergraded polymer remains high enough for the asymptote to be followed.

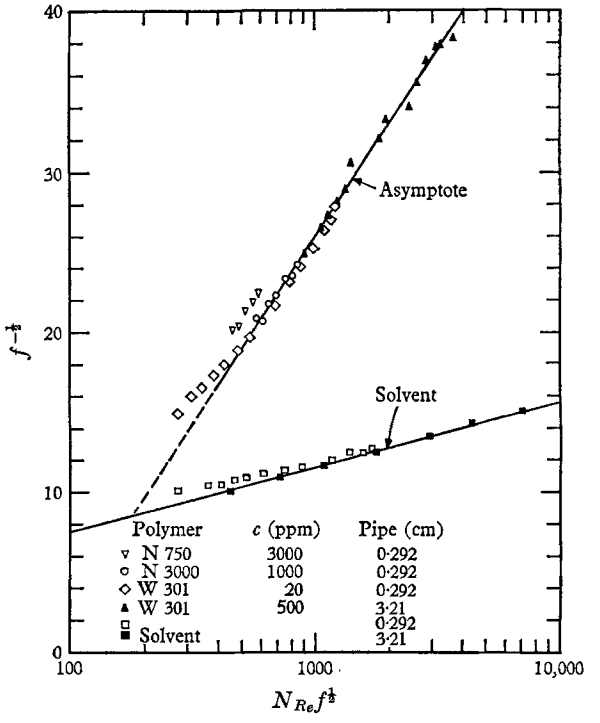

FIGURE 8. The maximum drag reduction asymptote. Solid lines for solvent and asymptote correspond to equations (20) and (24) respectively.

4. Results and discussion: flow structure

The polymer solution used for all flow structure measurements was 1000 ppm of N 3000.

The mean flow

Mean velocity profiles were measured in polymer solution at two flow rates: the 'low' flow rate was at onset, $(Q/Q^*) = 1$, $R_F \simeq 0$, while the 'high' flow rate was well into region (iv), $(Q/Q^*) = 5$, $R_F \simeq 0{\cdot}35$; flow conditions are summarized in table 4. The results, compared with identical measurements in solvent are shown in figures 9 and 10. On these, ξ is the normalized radial co-ordinate measured from the wall, U is the local axial mean velocity, U_{CL} is U at $\xi = 1{\cdot}0$ (the pipe centre line) while $u^+ = (U/u_\tau)$ and $y^+ = (\xi D u_\tau/2\nu)$ are the usual 'law of the wall' co-ordinates. Flow rates obtained by integration of the velocity profiles, Q_i, are

compared with those from the independent pump calibration, Q (with both solvent and polymer solution, the pump calibration was the same), in table 4. At both flow rates, Q_i and Q check comparably—indicating equal measurement accuracy—in polymer solution and solvent. To achieve this, a large diameter

Fluid	Q (l./sec)	Q_i (l./sec)	N_{Re}	R_F	u_τ (cm/sec)	V_S (cm/sec)	Pitot (cm)
Solvent	1·151	1·158	50,000	0	7·31	0	0·025
Polymer solution	1·148	1·137	36,000	0	7·42	0	0·025
Solvent	5·71	5·45	250,000	0	30·1	0	0·168
Polymer solution	5·71	5·55	180,000	0·35	25·0	160	0·168

Polymer solution is 1000 ppm of N 3000 in all cases.
Q_i is the flow rate obtained from velocity profile integration.
V_S is the 'effective slip' velocity, equation (18).

TABLE 4. Conditions for mean flow measurements (figures 9, 10, 11).

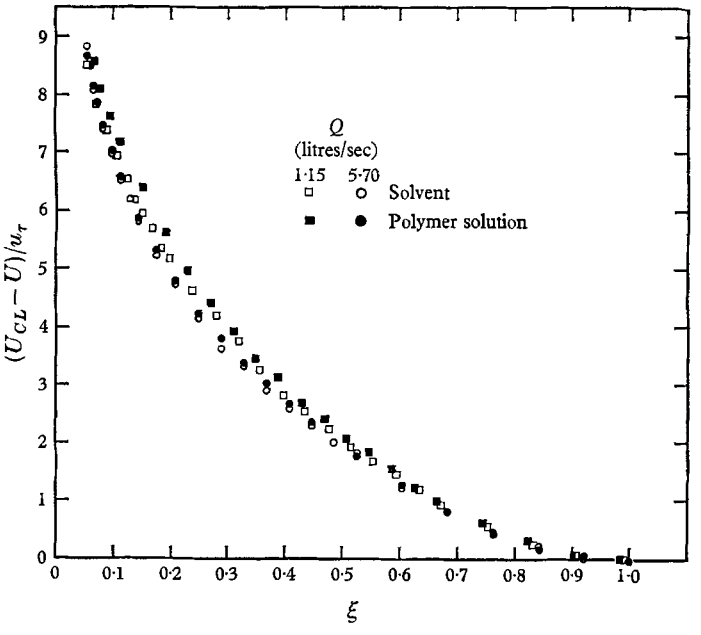

FIGURE 9. Velocity defect plots at two flow rates in 3·21 cm pipe (see table 4 for flow conditions).

0·168 cm Pitot tube had to be used to eliminate the 'discrepancy' observed in polymer solutions (Astarita & Nicodemo 1966; Smith, Merrill, Mickley & Virk 1967). With it the results were 1–2 % lower than with the 0·025 cm Pitot, but the error was the same in polymer solution and solvent so comparisons were not impaired.

At the low flow rate the solvent velocity defect and wall laws are obeyed quite precisely in polymer solution. At the high flow rate the solvent defect law,

figure 9, is obeyed closely, but the law of the wall, figure 10, is not—polymer solutions results are displaced upwards such that the slope (i.e. the mixing length constant) is essentially unchanged. Since u_τ in polymer solution is about 20 % lower, the obedience of the defect law indicates that values of $(U_{CL}-U)$ must everywhere be 20 % lower than in solvent and therefore that a distinctly blunter profile prevails when drag reduction is exhibited. Further, this shows that u_τ is a relevant velocity scale in polymer solutions. Together with the constancy of the mixing length constant, this implies that the profile in polymer solution is Newtonian when considered relative to U_{CL}—crudely speaking, when looked at from the top. This motivates the 'effective slip' model.

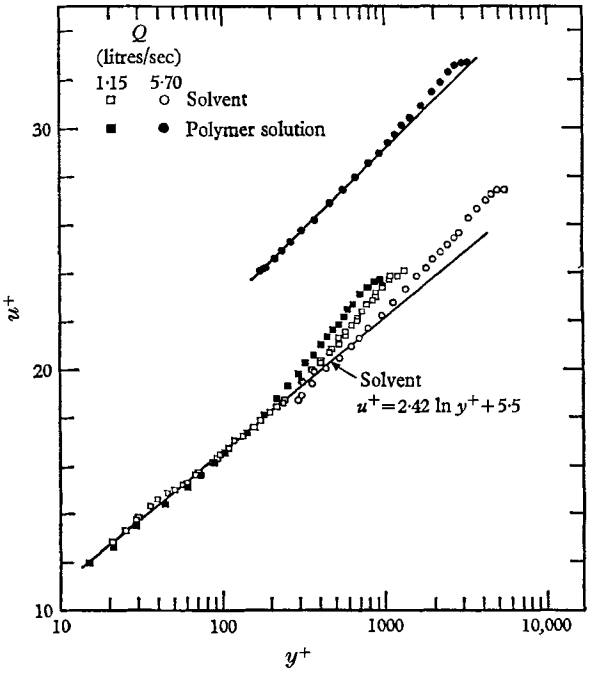

FIGURE 10. The law of the wall. Same conditions as for figure 9.

The effective slip model

At any point (Q, T_w) in fully developed turbulent flow, the mean velocity profile, $U(\xi)$, in dilute polymer solution consists of two additive portions or 'plugs':

(i) the profile, $V(\xi)$, that would exist in the Newtonian solvent at the prevailing wall shear stress, $T_w = \rho u_\tau^2$;

(ii) the constant 'effective slip' velocity, V_S, required to make up the difference between the actual average velocity, U_{av} (or flow rate, Q), and that, V_{av} (or flow rate, Q_N), obtained from integration of the Newtonian plug.

Thus at any radial position,

$$U(\xi) = V(\xi) + V_S, \tag{17}$$

where

$$V_S = U_{\mathrm{av}} - V_{\mathrm{av}} \tag{18}$$

and average velocities are defined in the usual way, e.g.

$$U_{\mathrm{av}} = \int_0^1 U d(1-\xi)^2 = 4Q/\pi D^2. \tag{19}$$

In the present case, $U(\xi)$, U_{av} and u_τ are known, so if the model holds, $V(\xi)$ should obey all Newtonian (i.e. solvent) laws. By definition (17), $V(\xi)$ will identically obey the same defect law as $U(\xi)$ which has already been noted to be Newtonian. Obedience of the wall law is tested as follows. If $V(\xi)$ is Newtonian, then V_{av} is available from u_τ via the Prandtl friction factor relation

$$f^{-\frac{1}{2}} = (V_{\mathrm{av}}/\sqrt{2}\,u_\tau) = 4{\cdot}0 \log_{10}(N_{Re} f^{\frac{1}{2}}) - 0{\cdot}4. \tag{20}$$

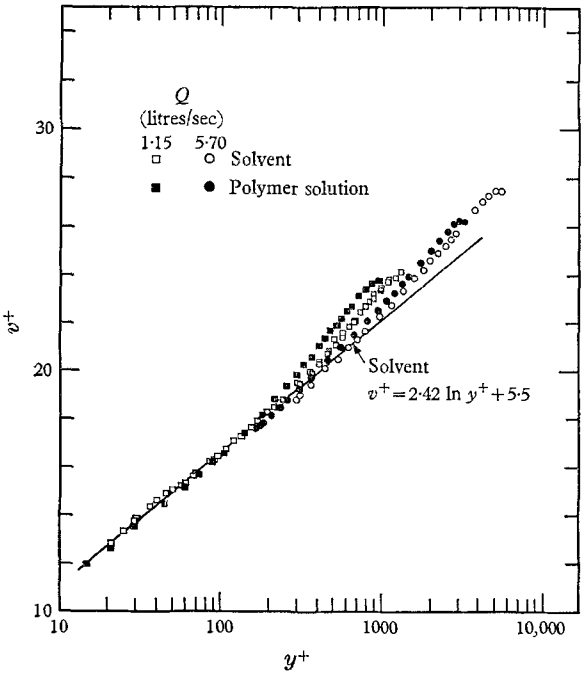

FIGURE 11. The law of the wall in the 'Newtonian plug' of the 'effective slip' model.

From V_{av} and (17) and (18), the $V(\xi)$ profile is obtained, point by point, from the $U(\xi)$ profile, and v^+ $(= V/u_\tau)$ *vs.* y^+ should be the same as for solvent. At the low flow rate, in general before onset, $V_S = 0$ so $V(\xi) \equiv U(\xi)$ and a purely Newtonian profile is predicted—as observed. v^+ *vs.* y^+ at the high flow rate is shown on figure 11 (compare figure 10)—the polymer solution points come within 1 % of the solvent, indicating good agreement with the model.

Physically, an actual slip at the wall is highly unlikely. The 'effective slip' is best considered the net result of processes occurring extremely close to the pipe wall, an interpretation made in direct analogy to the 'two-layer' concept for turbulent boundary layers (Clauser 1956). By this, the mean flow consists of an 'inner' region, say $0 < \xi < 0{\cdot}15$, which is directly governed by wall processes and an 'outer' region, say $0{\cdot}05 < \xi < 1{\cdot}00$, which is controlled only by conditions at

its boundaries and is, therefore, only loosely coupled to the wall processes in as much as they determine its inner boundary condition. In a fully developed pipe flow, the shear stress profile is linear in radius, so the shear stress 'seen' by the outer region at its inner edge is very close to the wall shear stress, T_w, hence, in it, u_τ is the velocity scale. Obedience to the 'effective slip' model indicates, therefore, that the outer region remains Newtonian even in flows exhibiting drag reduction. The outer region typically extends down to $y^+ \simeq 50$, so, by inference, the central differences between drag-reducing Toms phenomenon flows and true Newtonian flows must be in a region $0 < y^+ < 50$, extremely close to the pipe wall. This is also the region one would expect, intuitively, to be altered when there is drag reduction since it is where the energy production and dissipation rates are greatest.

Observe finally that the outer region comprises the entire flow save for a thin wall region: thus the 'effective slip' model is quite satisfactory for practical mean velocity profile prediction. Unfortunately no reliable mean velocity profiles have been reported in the literature so an independent check of the 'effective slip' model is lacking.

Turbulence structure

Turbulence measurements in polymer solution were made only at the high flow rate; their absolute accuracy is poorer than in solvent because the Newtonian heat transfer laws that the anemometer was designed for do not hold in polymer solution (Smith *et al.* 1967). Pertinent flow data is given in table 5.

Turbulent intensity profiles

In solvent, the rms axial turbulent velocity, u, could be measured to within $\pm 10\,\%$ and turbulent intensity profiles, $(u/u_\tau)\,vs.\,\xi$, agreed with established results (Laufer 1954). In polymer solution, figure 12, intensities (absolute value good to $\pm 20\,\%$) are essentially the same as solvent for $\xi < 0{\cdot}4$ but are higher for $0{\cdot}4 < \xi < 1.0$, with a maximum difference of $+20\,\%$ on the pipe axis; also there appears to be a 'plateau' for $0{\cdot}4 < \xi < 0{\cdot}7$. From the integrated momentum equation in a Newtonian flow,

$$(1-\xi)T_w = \rho\overline{u'v'} + (2\eta/D)\,(dU/d\xi), \tag{21}$$

so the local shear stress (LHS) is composed of turbulent, $\rho\overline{u'v'}$, and direct viscous components; u' and v' being the axial and radial turbulent velocities respectively. From the mean flow, for $y^+ > 50$, the viscous term, $(2\eta/D)\,(dU/d\xi)$, is that which would prevail in the Newtonian solvent at the same T_w, therefore $\rho\overline{u'v'}$ must also be. Thus, both (u/u_τ) and $\rho\overline{u'v'}$, in polymer solution follow Newtonian rules for $y^+ > 50$, $\xi < 0{\cdot}4$. In the central core, $0{\cdot}4 < \xi < 1.0$, which is relatively isotropic, one would expect v' to behave as u' so that, since $\rho\overline{u'v'}$ is still the same but u' considerably higher, it is likely that the correlation coefficient between u' and v' in polymer solution is reduced relative to the Newtonian plug—i.e. u' and v' are more out-of-phase. The physical significance of the intensity 'plateau' from $0{\cdot}4 < \xi < 0{\cdot}7$ is uncertain.

Energy spectra

One-dimensional turbulent energy spectra, $E_1(k_1)$ *vs.* k_1 in solvent and polymer solution are shown on figure 13 (*a*) and (*b*); the subscript 1 denotes the axial direction. Considerable confidence can be placed in spectra shapes—the distortion is about $\pm 5\,\%$—but the absolute value of the ordinate is $\pm 25\,\%$ in solvent

Fluid	Q (l./sec)	N_{Re}	R_F	u_τ (cm/sec)	ν (cm²/sec)
Solvent	5·30	234,000	0	28·4	0·00894
Polymer solution	5·70	180,000	0·25 ± 0·05	26·5 ± 1·0	0·0127

TABLE 5. Conditions for turbulence measurements (figures 12, 13).

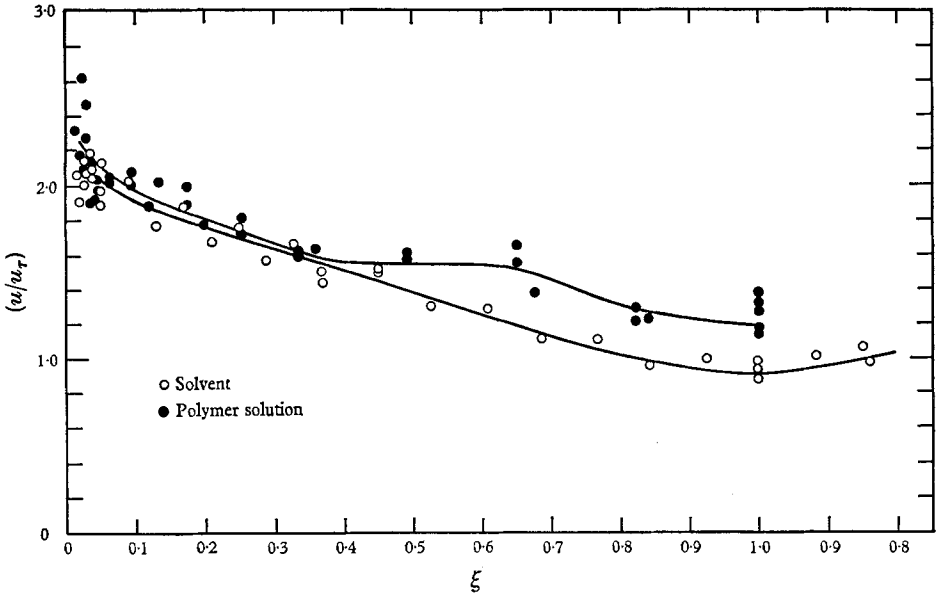

FIGURE 12. The rms turbulent intensity profiles, $N_{Re} \sim 200{,}000$, in 3·21 cm pipe (see table 5 for flow conditions).

and $\pm 50\,\%$ in polymer (this latter must be compared, however, with the 8 decade range spanned). Spectrum parameters are listed in table 6; Λ_f is the macroscale, characteristic of the large 'energy containing' eddies,

$$\Lambda_f = (\pi/2u^2)\, E_1(k_1)_{k_1 \to 0}, \tag{22}$$

ϵ_i is the dissipation rate assuming isotropy,

$$\epsilon_i = 15\nu \int_0^\infty k_1^2 E_1(k_1)\, dk_1, \tag{23}$$

and k_d is the dissipation wave-number defined in connexion with the Onset Hypothesis.

On the pipe axis, $\xi = 1{\cdot}00$, there is a distinct difference in spectra shapes; in particular the inertial subrange with slope roughly $-\frac{5}{3}$ that occurs for $2 < k_1 < 20\,\mathrm{cm}^{-1}$ in solvent is entirely absent in polymer solution in which, instead, there is an abrupt change in slope from $-\frac{2}{3}$ to -4 at $k_1 = 6\,\mathrm{cm}^{-1}$. Ideally, the inertial subrange is observed when the regions of turbulent energy production (predominantly low wave-numbers) and dissipation (predominantly

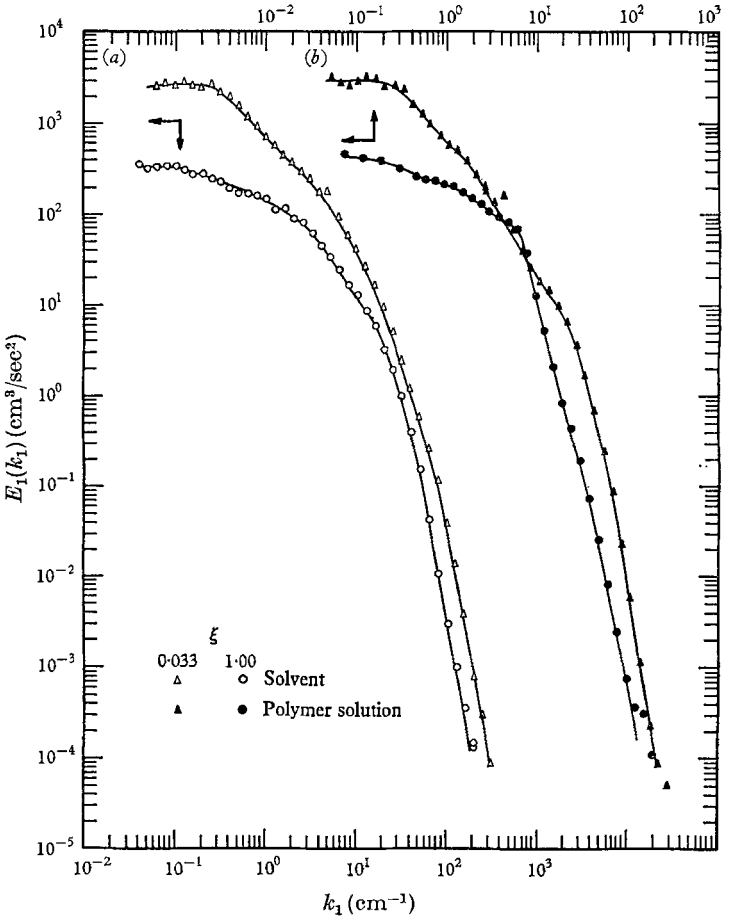

FIGURE 13. Axial turbulent energy spectra at two radial positions.

Fluid	ξ	u (cm/sec) rms	U (cm/sec)	Λ_f (cm)	ϵ_i (cm²/sec³)	k_d (cm⁻¹)
Solvent	1·00	27·0	765	0·73	8100	16
Polymer solution	1·00	32	822	0·77	4800	6
Solvent	0·033	59·5	500	1·15	26,000	16
Polymer solution	0·033	55	580	1·50	23,000	21

TABLE 6. Spectrum parameters.

high wave-numbers) are sufficiently separated; so its absence is indicative of smaller separation or of stronger coupling between these regions. From the experimental equality of the macroscales, Λ_f, the normalized energy density at the lower, energetic, wave-numbers is unchanged in polymer solution. It follows that the stronger coupling must result in the dissipative wave-numbers moving toward the origin; and, since dissipation varies as k_1^2; this must result in lower dissipation. Both these consequences are observed; from table 6, k_d decreases from 16 to 6 cm^{-1} and the dissipation in polymer solution is 40 % lower despite the turbulent kinetic energy, u^2, being 40 % higher than solvent.

Near the pipe wall, $\xi = 0{\cdot}033$, there is essentially no difference in the spectra; the shapes are remarkably similar, the ordinates only slightly different and the dissipation about 10 % less in polymer solution. This radial location corresponds to $y^+ \simeq 100$ which is still in the outer region, relatively remote from the energy action ($y^+ \simeq 10$).

Both intensity profiles and spectra exhibit the same behaviour. Near the wall (but still in the outer region), $y^+ > 50$, $\xi < 0{\cdot}4$, the intensity, (u/u_τ), turbulent shear stress, $\rho\overline{u'v'}$, and axial spectra indicate a Newtonian turbulence structure in polymer solution, strongly reinforcing the notion of a Newtonian plug convected along intact at an additional, 'effective slip' velocity. Towards the pipe axis, the turbulence structure is distinctly different from Newtonian. Note, however, that Newtonian scaling fails only at the highest echelon of detail—turbulence structure—and then only in the central core, which region is the least dominated by the energy processes occurring near the wall. Since these energy processes are of the greatest interest *vis-à-vis* drag reduction, it is possible that the turbulence structure in the central core is due to causes not directly related to those causing the Toms phenomenon, though both must, eventually, be traced to the addition of macromolecules.

5. Conclusions

Evaluation of earlier explanations

Of the four types of explanations cited earlier (§ 1), the inherent transition delay (ii), is definitely not valid since transition is not generally delayed. 'Effective slip', (i), is well obeyed, which shows that the significant differences between Toms phenomenon and true Newtonian flows lie in the immediate vicinity of the wall, $0 < y^+ < 50$, but it remains a device which permits convenient computation without regard to the underlying molecular mechanism. In fact, the causes of the 'effective slip' are likely encompassed within the remaining two molecular types of explanations, (iii) and (iv). Because experimental measurements were not made in the immediate wall region, $0 < y^+ < 50$, no conclusive distinction can be made between the anisotropic viscosity and visco-elasticity explanations but the peripheral evidence available favours the latter.

Prediction of the Toms phenomenon

The present findings are summarized in the form of a generalized Toms phenomenon flow diagram, figure 14.

The three limiting lines are:

AB Poiseuille's law

$$f = 16N_{Re}^{-1}; \tag{15a}$$

DG Prandtl's universal turbulent friction factor law

$$f^{-\frac{1}{2}} = 4.0\log_{10}(N_{Re}f^{\frac{1}{2}}) - 0{\cdot}4; \tag{20}$$

EH the maximum drag reduction asymptote

$$f^{-\frac{1}{2}} = 23\log_{10}(N_{Re}f^{\frac{1}{2}}) - 43. \tag{24}$$

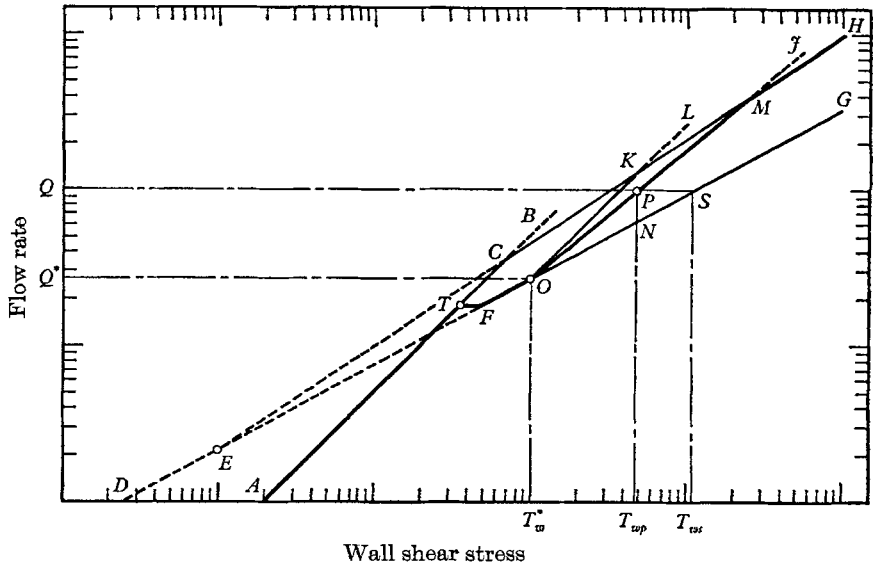

FIGURE 14. General Toms phenomenon flow diagram. Dashed lines indicate virtual regions, not physically attained.

The most general flow path is *ATFOMH* with segments:

AT laminar flow;

TF transition region with T, the transition point, at the same $N_{Re,T}$ as solvent;

FO fully developed turbulent flow, without drag reduction,

O onset point (Q^*, T_w^*) at which T_w^* is related to the polymer by the Onset Hypothesis

$$(D_M u_\tau^*/\nu) = 0{\cdot}015; \tag{25}$$

OM turbulent flow, with drag reduction, controlled by polymer parameters—concentration, molecular weight, species;

MH turbulent flow along maximum drag reduction asymptote independent of polymer.

Special cases

(i) $c \to \infty$, *ATFOKH* is followed, the polymer solution flow line *OM* tending to asymptote *OK*, the slope of which, *Np*, depends on polymer.

(ii) $T_w^* < T_{w,T}$, segment *FO* is absent, drag reduction being attained as soon as turbulent flow is established.

(iii) $T_w(M) < T_w(C)$, if the point M is predicted to lie to the left of point C, i.e. in a 'virtual' region, then the maximum drag reduction asymptote will be followed—path ACH—independent of polymer and concentration.

Mean velocity profiles

At any point, $P(Q, T_w)$, in fully developed turbulent flow the corresponding Newtonian 'plug' refers to point $N(Q_N, T_w)$ on the Newtonian solvent line. The 'effective slip' velocity is

$$V_S = U_{\text{av}} - V_{\text{av}} = 4(Q - Q_N)/\pi D^2. \tag{18}$$

Equally, V_{av} is available from T_w and (20). The Newtonian 'plug' profile, $V(\xi)$, at N is obtained from standard u^+ *vs.* y^+ relations (see e.g. Hinze 1959). The required velocity profile $U(\xi)$, is the addition of $V(\xi)$ and V_S (equation (17)), valid only in the 'outer region', $y^+ > 50$.

Turbulence structure

Turbulence measurements were made at a single flow rate so the conclusions are qualitative. When drag reduction is exhibited, the turbulence structure in the outer region ($y^+ > 50$) tends to follow the effective slip model towards the wall but deviates markedly from this in the central core of the pipe. In particular, on the axis, the turbulent intensity is higher than Newtonian and the inertial subrange, characteristic of Newtonian energy spectra (Laufer 1954), is absent in the polymer solution.

This work was supported by the Office of Naval Research under Contract Number 3963 (10).

REFERENCES

ASTARITA, G. & NICODEMO, L. 1966 Velocity distributions and normal stresses in visco-elastic turbulent pipe flow. *A.I.Ch.E. J.* **12**, 478.

CLAUSER, F. H. 1956 The turbulent boundary layer, in *Advances in Applied Mechanics*, H. L. Dryden and Th. von Kármán, Ed., vol. IV, p. 1. New York: Academic Press.

FABULA, A. G. 1963 The Toms Phenomenon in the turbulent flow of very dilute polymer solutions. *4th Int. Congress on Rheology, Brown U., Providence, Rhode Island.*

FLORY, P. J. 1953 *Principles of Polymer Chemistry*. Ithaca, New York: Cornell University Press.

HERSHEY, H. C. & ZAKIN, J. L. 1965 A study of turbulent drag reduction of solutions of high polymers in organic solvents. *Preprint 21B, Symposium on Mechanics of Visco-elastic Fluids, Part II, 58th Meeting, A.I.Ch.E., Philadelphia, Pa.*

HINZE, J. O. 1959 *Turbulence*. New York: McGraw-Hill.

LAUFER, J. 1954 The structure of turbulence in fully developed pipe flow. *NACA Rept.* no. 1174.

METZNER, A. B. & PARK, M. G. 1964 Turbulent flow characteristics of visco-elastic fluids. *J. Fluid Mech.* **20**, 291.

OLDROYD, J. G. 1948 A suggested method of detecting wall effects in turbulent flow through pipes. *Proc. 1st Int. Congress on Rheology*, vol. II, pp. 130–4. North Holland Publ. Co.

PETERLIN, A. 1960 Gradient dependence of intrinsic viscosity of freely flexible linear macromolecules. *J. Chem. Phys.* **33**, 1799.

SAVINS, J. G. 1964 Drag reduction characteristics of solutions of macromolecules in turbulent pipe flow. *Soc. Petrol. Eng. J.* **4**, 203.

SHIN, H. 1965 *Reduction of Drag in Turbulence by Dilute Polymer Solutions*. Sc.D. Thesis, M.I.T., Cambridge, Mass.

SMITH, K. A., MERRILL, E. W., MICKLEY, H. S. & VIRK, P. S. 1967 Anomalous Pitot tube and hot film measurements in dilute polymer solutions. *Chem. Engng Sci.* **22**, 619.

TANFORD, D. 1961 *The Physical Chemistry of Macromolecules*. New York: John Wiley.

TOMS, B. A. 1948 Some observations on the flow of linear polymer solutions through straight tubes at large Reynolds numbers. *Proc. 1st Int. Congress on Rheology*, vol. II, pp. 135–41. North Holland Publ. Co.

VIRK, P. S., MERRILL, E. W., MICKLEY, H. S. & SMITH, K. A. 1965 The Critical wall shear stress for reduction of turbulent drag in pipe flow, in *Modern Developments in the Mechanics of Continua*, S. Eskanazi, Ed. New York: Academic Press.

VIRK, P. S. 1966 *The Toms Phenomenon–Turbulent Pipe Flow of Dilute Polymer Solutions*. Sc.D. Thesis, M.I.T., Cambridge, Mass.

ZIMM, B. H. 1956 Dynamics of polymer molecules in dilute solutions: viscoelasticity, flow birefringence and dielectric loss. *J. Chem. Phys.* **24**, 269.